RSC Advances

PAPER

View Article Online
View Journal | View Issue

Cite this: *RSC Adv.*, 2025, **15**, 23827

Synthesis of C_{60}-CM-C_n and its effect on the stabilization of nitrocellulose†

Haoxi Chu, Bo Jin, * Yang Zhao and Rufang Peng*

Received 11th March 2025
Accepted 2nd June 2025

DOI: 10.1039/d5ra01741f

rsc.li/rsc-advances

The fullerene derivative C_{60}-CM-C_n was synthesized *via* a two-step reaction using fullerene (C_{60}), curcumin ($C_{21}H_{18}O_5$), and bromoalkanes (RBr) as raw materials. The structure of C_{60}-CM-C_n was characterized by nuclear magnetic resonance (^{1}H and ^{13}C NMR) and high-resolution mass spectrometry (HR MS). Thermal analysis, including differential thermal analysis (DTA), vacuum stability tests (VST), thermogravimetric analysis (TG), and methyl violet experiments, along with electron paramagnetic resonance spectroscopy, was used to investigate the interaction mechanism between C_{60}-CM-C_n and nitrocellulose (NC). The results demonstrated that there is good compatibility between C_{60}-CM-C_n and NC, C_{60}-CM-C_n extended the color change time of methyl violet paper by 28–47 min, reduced the gas released during the thermal decomposition of NC by 0.7–1.69 mL g^{-1}, and decreased the heat loss rate of NC by 9.8–15.6%. Additionally, at a minimum concentration of 0.19 g L^{-1}, C_{60}-CM-C_n achieved a 50% removal rate of nitrogen oxides (NO_x). These findings indicate that C_{60}-CM-C_n serves as an effective antioxidant for the removal of nitrogen oxides from NC fibers, outperforming traditional stabilizers such as diphenylamine (DPA) and C2 in improving NC stability.

1. Introduction

Solid propellants with nitrate compounds as the main components have gained widespread use due to their high energy content and reduced smoke signature.[1,2] However, due to the low dissociation energy of nitrate bonds, these compounds are prone to decomposition, which may occur during storage and transportation. And the decomposition process releases nitrogen oxides and nitrogen oxygen radicals, which further catalyze the decomposition of nitrate and generate excessive heat, ultimately affecting the performance of solid fuels. To extend the service life of solid propellants and pyrotechnic explosives, small amounts of chemical stabilizers are added to absorb the nitrogen oxides generated by nitrate decomposition, thereby inhibiting autocatalytic decomposition.[3–6]

Traditional stabilizers are primarily classified into aniline and phenylurea derivatives,[7,8] such as diphenylamine (DPA), 2-nitrodiphenylamine (2-NDPA), *N*-methyl-*p*-nitroaniline (MNA), *N*,*N*′-diethyl-*N*,*N*′-diphenylurea (C1), *N*,*N*′-dimethyl-*N*,*N*′-diphenylurea (C2), 1,1-diphenylurea (AKI), and 3-methyl-1,1-diphenylurea (AKII). DPA, 2-NDPA, and MNA are chemically basic and can absorb nitrogen-oxygen acid gases, chemically inhibiting the autocatalytic decomposition of nitrocellulose and improving fuel stability.[9,10] However, the strong alkalinity of aniline-based stabilizers can promote the saponification reaction of nitrate, reducing the chemical stability of the propellant.[11,12] Phenylurea-based stabilizers, such as C1, C2, AKI, and AKII, reduce the strength of amine-based stabilizers due to the strong electron-withdrawing effect of the carbonyl group. This effect reduces the alkalinity of the amine group, effectively inhibiting the saponification of nitrate groups but also decreasing the scavenging ability for NO_x.[13,14] Moreover, traditional stabilizers generally exhibit poor scavenging capacity for nitrogen and oxygen radicals, making it critical to develop a chemical stabilizer capable of absorbing both nitrogen oxides and free radicals.

Fullerenes, known as "free radical sponges", possess unique three-dimensional hollow structures, high antioxidant and acid corrosion resistance, good thermal stability, and effective scavenging abilities for various free radicals in the environmental system. They also exhibit good compatibility with other major components in propellants, making them ideal materials for chemical stabilizers.[15–18] It has been demonstrated that the scavenging of various free radicals (*e.g.*, hydroxyl and superoxide radicals) can be enhanced by introducing external groups through chemical modification of fullerenes.[19,20] Based on this, a series of new fullerene cyclopropane and pyrrolidine derivatives with dual-function stabilizers were synthesized by combining fullerenes with traditional stabilizers at the molecular level using functional derivatization methods such as Bingel, Prato, and F–C reactions. These new derivatives were evaluated for their ability to absorb free radicals, and the results showed that the stabilization effect of fullerenes on NC was significantly better than that of DPA and C2.[21–25]

State Key Laboratory of Environment-friendly Energy Materials, Southwest University of Science and Technology, Mianyang 621010, China. E-mail: jinbo0428@163.com; rfpeng2006@163.com

† Electronic supplementary information (ESI) available. See DOI: https://doi.org/10.1039/d5ra01741f

However, research on fullerene stabilizers remains limited, and there is no clear understanding of the conformational relationship between small molecule structures and fullerenes. Recent studies have shown that the natural compound curcumin can also serve as a stabilizer to inhibit the autocatalytic degradation process that produces nitrous gas and free nitric acid.[26,27] To further study the molecular structure of fullerene materials and their free radical scavenging capabilities, as well as their stabilizing effect on NC, this study synthesized C_{60}-CM-C_n *via* a two-step reaction using fullerene, the natural small molecule curcumin, and bromoalkanes as raw materials. The influence of the synthesized compound on NC and its potential as a stabilizer for double base propellants were evaluated using methods such as DTA, isothermal thermogravimetric analysis, methyl violet test, and ESR.

2. Experimental

2.1. Synthetic procedures

2.1.1. Materials. C_{60} (99.5% purity) was obtained from Puyang Yongxin Fullerene Technology Co., Ltd. Curcumin, (analytical pure) was sourced from Shanghai Yi En Chemical Technology Co., Ltd. Carbon tetrabromide (99%) was purchased from Shanghai Merrill's Reagent. DPA, 3-methyl-1, 1′-diphenylurea, and 1, 8-diazabicyclo[5.4.0]undec-7-ene were examined alongside potassium iodide (99%, Shanghai Aladdin Reagent). Sodium nitroprusside, sodium diethyldithiocarbamate trihydrate, ethyl bromide, propyl bromide, butyl bromide, and benzyl bromide were all obtained in analytical purity from Shanghai Maclean's Biochemical Science and Technology. Additional materials included 300–400 mesh silica gel, anhydrous ethanol, *n*-hexane, toluene, carbon disulfide, methylene chloride, *o*-dichlorobenzene, ferrous sulfate heptahydrate, and anhydrous potassium carbonate (all analytical grade from Chengdu Kelon Chemical Reagent). Methyl violet test paper was sourced from the Xi'an Institute of Modern Chemistry.

2.1.2. Synthetic procedures. The synthetic routes of curcumin-derivatized small molecules and C_{60}-CM-C_n are shown in Fig. 1.

Curcumin (9.2 g, 0.025 mol), potassium carbonate (13.8 g, 0.10 mol), alkyl bromide (0.10 mol), and potassium iodide (1.7 g, 0.01 mmol) were combined in 80 mL of ethanol. The mixture was heated, condensed, and refluxed for 48 h to facilitate the reaction. Afterward, the mixture was filtered and concentrated, yielding a brown solid product (curcumin-derivatized small molecules **1a–d** (ref. 28)). In a separate process, 360 mg (0.5 mmol) of C_{60} was weighed into a 50 mL single-necked round-bottom flask. To this, 10 mL of *o*-dichlorobenzene was added, and the mixture was sonicated until the C_{60} fully dissolved. Next, 446 mg (1.5 mmol) of carbon tetrabromide, 150 μL of 1,8-diazabicyclo[5.4.0]undec-7-ene, and 500 mg of products **1a–d** were introduced. The reaction was stirred for an hour and a half at room temperature. Upon completion, the product was purified *via* silica gel column chromatography. The brown products **2a–d** were collected through gradient elution with toluene-dichloromethane, resulting in reddish-brown solutions that were spun-dried to yield the final brown products. The structures of the products were characterized using ^{1}H NMR, ^{13}C-NMR, and high-resolution mass spectrometry (HRMS).

2.2. Equipment and conditions

2.2.1. Preparation of the NC stabilizers samples. 15 mg of various stabilizers (DPA, C2, **2a–d**) were dissolved in 10 mL of

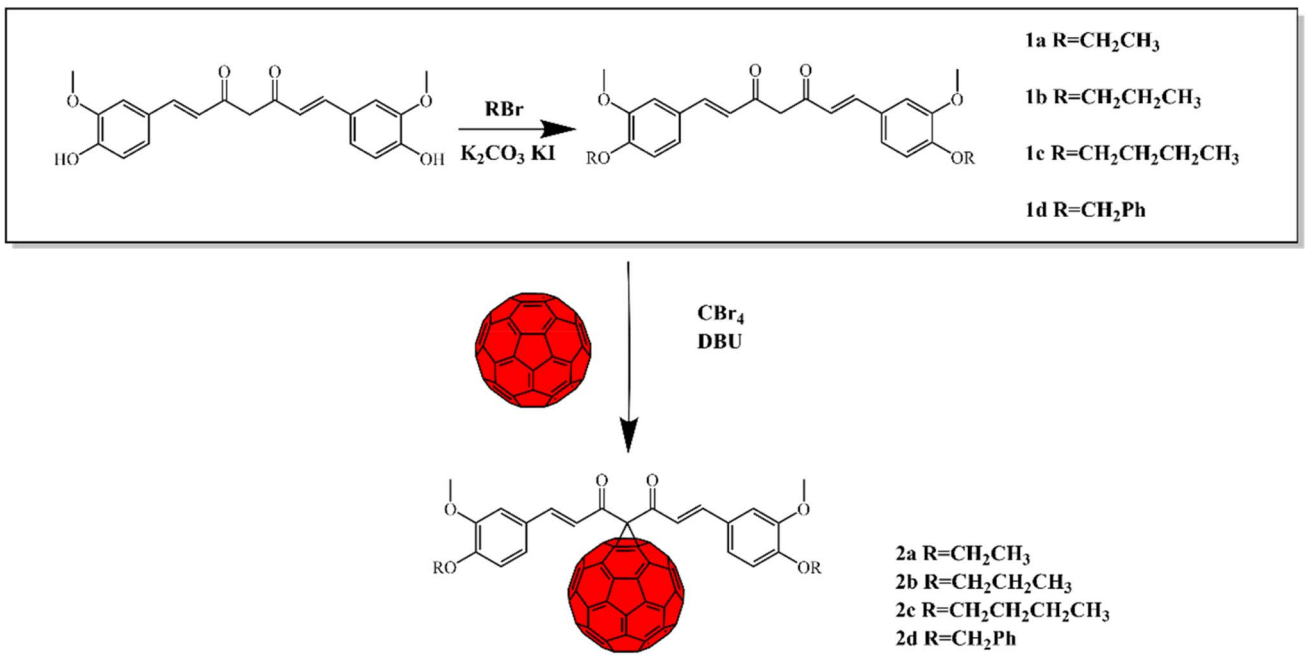

Fig. 1 Synthetic routes for C_{60}-CM-C_n.

Table 1 Basic formulations of NC stabilizers samples

		wt/%	
Samples	Stabilizers	NC/NG	Stabilizers
S-1	None	100	0
S-2	DPA	97	3
S-3	C2	97	3
S-4	**2a**	97	3
S-5	**2b**	97	3
S-6	**2c**	97	3
S-7	**2d**	97	3

carbon disulfide. Subsequently, 485 mg of NC was added, and the mixture was stirred with a glass rod until the solvent evaporated completely, ensuring uniform dispersion of the stabilizers on the surface of the NC. This resulted in a homogeneous sample mixture (stabilizer/NC). The mixed sample was then vacuum dried at 45 °C for 48 h until it reached a constant weight, producing the final sample, as outlined in Table 1.

2.2.2. DTA test. For thermal decomposition performance testing, a mixed sample of 1.50 mg pure NC and C_{60}-CM C_n/NC with a mass ratio of 1 : 1 was heated from 40 °C to 300 °C at a rate of 10 °C min^{-1}. The decomposition peak temperature was recorded and compared to evaluate the compatibility of C_{60}-CM C_n with NC.

2.2.3. Methyl violet test. The methyl violet experiment was conducted using the VDY00-01 device at 134.5 °C with a sample mass of 300 mg. The time taken for the methyl violet test paper to change from purple to orange-red was documented.

2.2.4. Vacuum stability test (VST). Gas volume release was measured at 100 °C over a duration of 48 h with a sample mass of 100 mg. The amount of gas released was recorded post-experiment.

2.2.5. TG test. Under the experimental conditions of a nitrogen-flowing atmosphere (40 mL min^{-1}), a temperature of 134.5 °C, a constant temperature duration of 6 h, and a sample mass of 3.2 mg, a weight loss experiment was conducted using a 404 F1 differential scanning calorimeter (Netzsch). The weight loss rate of the sample was recorded.

2.2.6. ESR test. The ESR test was performed using a Bruker-EMXnano instrument with a sweep width of 150.0 G, a center magnetic field of 3373.05 G, and a sample *g*-factor of 2.0400. The auxiliary reagents used were sodium nitroprusside (SNP) at 2 mM, $FeSO_4 \cdot (H_2O)_7$ at 20 Mm, and sodium diethyldithiocarbamate trihydrate (DETC) at 40 mM. Fullerene derivatives were dissolved in CS_2 to prepare solutions with concentrations of 0.2, 0.4, 0.8, 1.6, and 3.2 mM.

3. Result and discussion

3.1. Structural characterization of fullerene derivatives

C_{60}-CM-C_n (**2a–d**) was synthesized as described previously. Compounds **2a–d** were analyzed using ^{1}H-NMR, ^{13}C-NMR, and HRMS (Fig. S1–S12†).

The ^{1}H NMR spectrum of compound **2a** displays a triple peak at δ 1.52 ppm for the six methyl protons in the ethyl branch chain. It also shows two double peaks at δ 4.22 ppm for the four methylene protons, a single peak at δ 4.01 ppm for the six methoxyl protons, and four double peaks at δ 6.95 ppm and

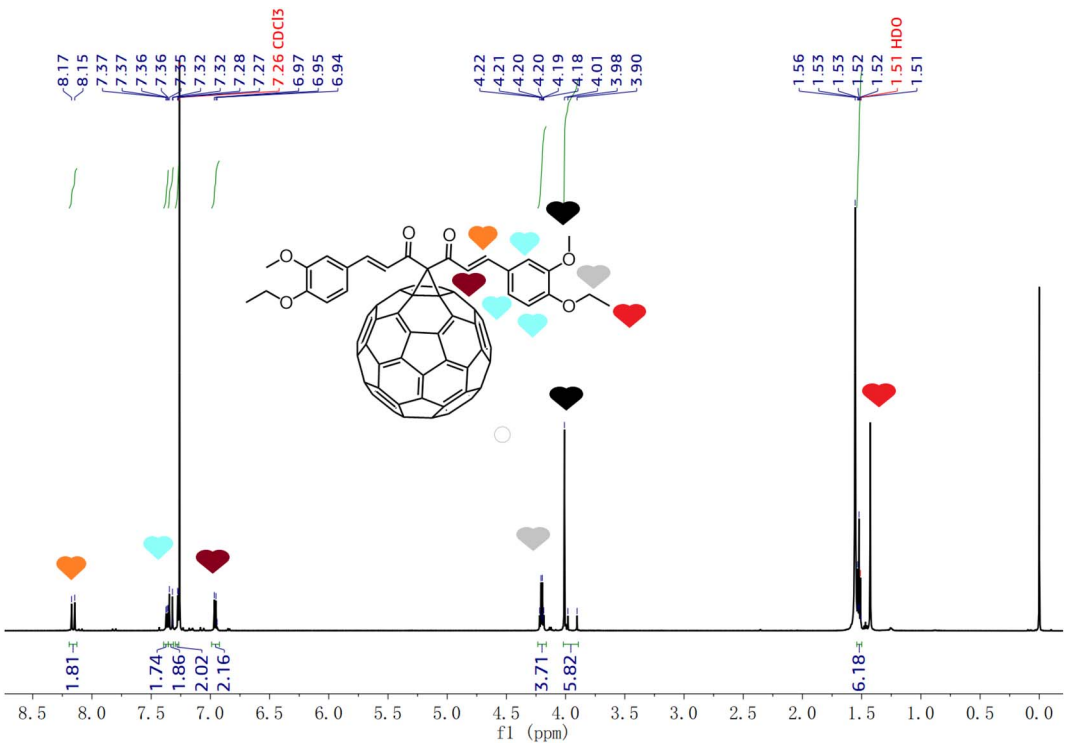

Fig. 2 ^{1}H NMR spectra of compound **2a**.

δ 8.16 ppm for the four protons on the double bond. The two benzene rings show double peak at δ 7.28 ppm, δ 7.32 ppm and δ 7.36 ppm for their six protons, respectively.[28–30] As depicted in Fig. 2, the ^{13}C NMR spectra indicate that the sp^2-C peaks on the fullerene carbon cage range from 140 to 150 ppm. The characteristic peak for carbonyl carbon appears at 186.95 ppm, while the sp^3-C peak attached to the external group is found at 70.80 ppm. The peaks corresponding to carbon atoms attached to the fullerene are at 46.78 ppm. The methoxyl carbon peak is at 56.27 ppm, and the ethyl carbon peaks are at 10.40 ppm and 22.35 ppm. Characteristic peaks for three carbon atoms attached to the external benzene ring are located at 110.91 ppm, 118.69 ppm, and 123.59 ppm. The carbon atoms connected to the carbon chain on the benzene ring show peaks at 126.61 ppm, while the peaks for carbon atoms bonded to the benzene ring and the two carbon atoms attached to the ethoxyl ring are found at 152.27 ppm. Peaks for carbon atoms connected to the double bond are detected at 137.40 ppm and 124.59 ppm.[31] The HRMS result of 1142.17 matches the expected molecular weight, confirming the target structure (Fig. S1–S3†).

The ^{1}H NMR spectra of compound **2b** reveal a triple peak at δ 1.05 ppm, indicating six methyl protons on the *n*-propyl group. There are two double peaks at δ 1.90 ppm and δ 4.92 ppm for eight methylene protons. A single peak at δ 4.01 ppm corresponds to six methoxyl protons, while four protons on the double bond show peaks at δ 6.93 ppm and δ 8.28 ppm. The six protons from the two benzene rings appears as two peaks at δ 7.22–7.24 ppm and δ 7.30–7.32 ppm. The ^{13}C NMR spectrum presents a characteristic peak for sp^2-C in the fullerene carbon cage, located between 140–150 ppm. There is also a notable carbonyl carbon peak at 186.13 ppm and a peak for fullerene sp^3-C linked to an external group at 74.26 ppm. Peaks for carbon atoms attached to fullerenes are found at 31.59 ppm, while methoxyl carbons appear at 56.45 ppm. The *n*-propyl carbon peaks are observed at 10.38 ppm, 22.31 ppm, and 71.06 ppm. There characteristic peaks for the carbons attached to the external benzene ring are identified at 110.73 ppm, 112.39 ppm, and 120.73 ppm. Additionally, peaks for the carbon atoms attached to the carbon chain on the benzene ring are located at 126.68 ppm. Two carbon atoms connected to the oxygen on the benzene ring are found at 152.40 ppm, and carbon atoms tied to the double bond appear at 137.81 ppm and 125.02 ppm. The HRMS result of 1170.20 aligns with the expected molecular weight, confirming the target structure (Fig. S4–S6†).

The ^{1}H NMR spectrum of compound **2c** reveals a triple peak at δ 0.97 ppm, corresponding to six methyl protons on the butyl group. Additionally, there are two double peaks at δ 1.50 ppm and δ 1.85 ppm, representing 12 protons from the three methylene groups. A double peak at δ 3.95 ppm indicates six methoxyl protons, while the double bond protons show peaks at δ 6.92 ppm and δ 8.28 ppm. The four protons in the double bond also exhibit two double peaks at δ 6.92 ppm and δ 8.16 ppm. The six protons on the two benzene rings are represented by three peaks at δ 7.23 ppm, δ 7.32 ppm, and δ 7.36 ppm. The ^{13}C NMR spectrum displays characteristic peaks of sp^2-C within the fullerene carbon cage, found in the range of 140–150 ppm. The carbonyl carbon appears at 185.29 ppm, and the fullerene sp^3-C connected to an external group shows a peak at 75.79 ppm. Peaks for carbon atoms attached to fullerenes are observed at 31.05 ppm. Methoxyl carbon is identified at 56.31 ppm, while *n*-butyl carbon peaks are seen at 13.84 ppm, 19.19 ppm, 26.93 ppm, and 68.86 ppm. Peaks corresponding to three carbon atoms on the benzene ring appear at 111.02 ppm, 112.43 ppm, and 118.73 ppm. Peaks for carbon atoms on the benzene ring attached to the carbon chain are found at 126.65 ppm. Two carbon atoms on the benzene ring connected to oxygen show peaks at 152.37 ppm, and double-bonded carbon atom are found at 137.43 ppm and 124.58 ppm. The HRMS result of 1198.23 matches the expected molecular weight, confirming the target structure (Fig. S7–S9†).

The ^{1}H NMR spectrum of compound **2d** displayed a single peak at δ 5.21 ppm for the four methylene protons in the two benzyl groups. There were also two multiplet peaks at δ 7.36–7.43 ppm for the ten protons on the benzene rings in the two benzyl groups. A single peak appeared at δ 3.95 ppm for the six methoxyl protons, while two double peaks were noted at δ 6.96 ppm for four protons on the double bond and at δ 7.61 ppm for six methoxyl protons. The six protons from the two benzene rings generated three peaks at δ 7.01 ppm, δ 7.12 ppm, and δ 7.26 ppm. The ^{13}C NMR spectrum indicated characteristic peaks of sp^2-C in the fullerene carbon cage occurring between 140–150 ppm. The carbonyl carbon appeared at 186.84 ppm, while the characteristic peaks of the fullerene sp^3-C attached to the external group were around 70.92 ppm. Peaks for carbon atoms bound to the fullerene ranged from 35.81 ppm, and methoxyl carbon appeared at 56.24 ppm. The benzylic carbon was observed between 127 ppm to 128.99 ppm, with another peak at 136.40 ppm and one at 57.33 ppm. The three carbon atoms on the benzene ring were found at 111.14 ppm, 113.49 ppm, and 121.66 ppm. The carbon atom linked to the carbon chain on the benzene ring appeared at 123.65 ppm, while the two carbon atoms attached to the oxygen on the benzene ring were identified at 151.27 ppm. The characteristic peaks for double-bonded carbons were recorded at 137.20 ppm and 129.66 ppm. The HRMS result of 1126.20 was consistent with the expected molecular weight, aligning with the target structure (Fig. S10–S12†).

3.2. Compatibility of C_{60}-CM-C_n with NC

The compatibility of NC with various stabilizers was assessed according to NATO standardization protocol STANAG 4147. The experimental design takes the change in thermal decomposition characteristic peak temperature (T_p) of nitrocellulose samples after adding 50% mass fraction stabilizer as the core judgment basis, and establishes the following compatibility grading standards: when the temperature deviation is in the range of 0–2 °C, it indicates that the stabilizer and nitrocellulose are in a completely compatible state; when the offset is 3–5 °C, it is determined to be partially compatible but slightly sensitive, and long-term storage is not recommended; when the offset range reaches 6–15 °C, it shows that the two are incompatible and the system is sensitive; if the temperature deviation exceeds

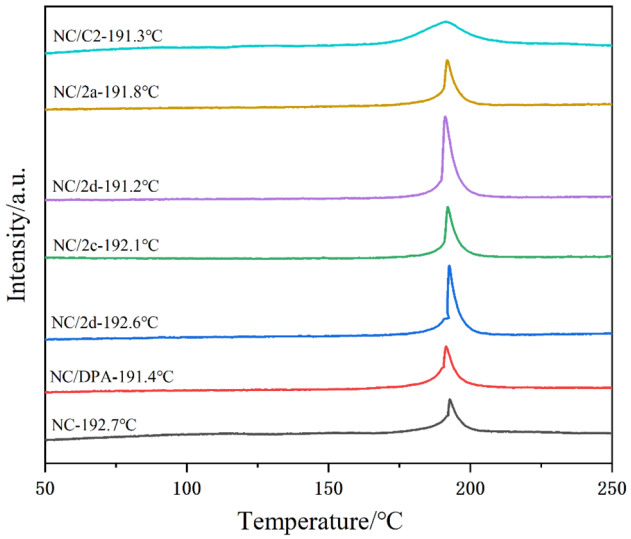

Fig. 3 DTA curves of the different stabilizer and NC mixtures.

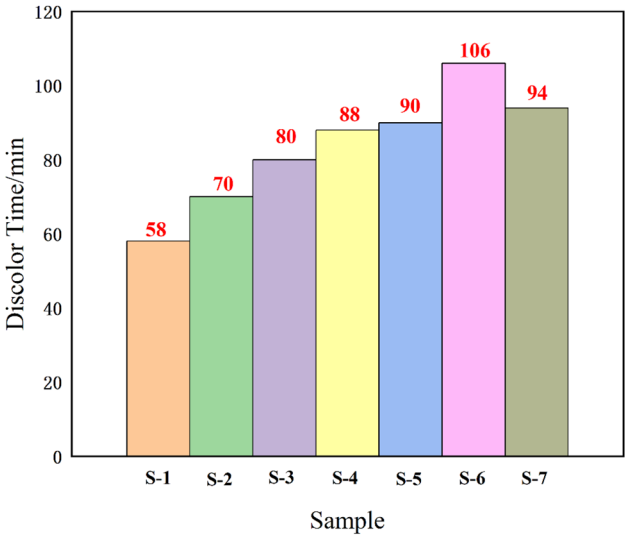

Fig. 4 Color change of samples in methyl violet test at 134.5 °C.

Table 2 Compatibility data of NC for DTA peak temperature

Samples	Decomposition temperature/°C	ΔT_p/°C	Compatibility level
NC	192.7	—	—
NC/DPA	191.4	1.3	Compatible
NC/C2	191.3	1.4	Compatible
NC/**2a**	191.8	0.9	Compatible
NC/**2b**	191.2	1.5	Compatible
NC/**2c**	192.1	0.6	Compatible
NC/**2d**	192.6	0.1	Compatible

15 °C, it indicates that the two are completely incompatible.[32–34] The compatibility of NC with C_{60}, DPA, C2, and compounds **2a–d** was evaluated through the DTA method. As shown in Fig. 3, the DTA curves for all samples featured a single decomposition peak, and the temperature difference in the exothermic peak for samples S1–S7 was only 2 °C. These results indicate good compatibility of **2a–d** with NC (Table 2).

3.3. Stabilization effect of C_{60}-CM-C_n

3.3.1. Methyl violet test. The stabilizing effect of the stabilizer was evaluated using the methyl violet test, where the time for the methyl violet test paper to change from violet to orange was measured. The nitrogen oxides produced by the thermal decomposition of NC cause the test paper to change color. The stabilizer absorbs these nitrogen oxide radicals, reducing the autocatalytic decomposition rate of NC and extending the color change time. Therefore, the discoloration time of the methyl violet test paper reflects the stabilizing effect of the stabilizer. The discoloration process and the times for each sample are shown in Fig. 3. The discoloration times for samples S-1 to S-7 were 58, 70, 80, 88, 90, 106, and 94 min, respectively. This indicates that the addition of fullerene derivatives delayed the discoloration time by 31 to 47 min. The order of discoloration times was S-6 > S-7 > S-5 > S-4 > S-3 > S-2 > S-1. Thus, the stabilizing ability of the stabilizers on NC follows the order **2c** > **2d** > **2b** > **2a** > C2 > DPA. The experimental results demonstrate that C_{60}-CM-C_n exhibits better stabilizing performance than both C2 and DPA (Fig. 4).

3.3.2. Vacuum stability test. The stabilizing effect of the stabilizer in the sample is determined by measuring the volume of gas produced by the decomposition of the sample per unit mass under experimental conditions. Under identical conditions, less gas released from the sample indicates a better stabilizing effect. The formula to estimate gas volume under standard conditions is:

$$V_H = 2.69 \times 10^{-3} P(V_0 - V_G)/T \quad (1)$$

where, the volume of gas released by the sample under standard conditions is expressed by V_H, the sample pressure is expressed

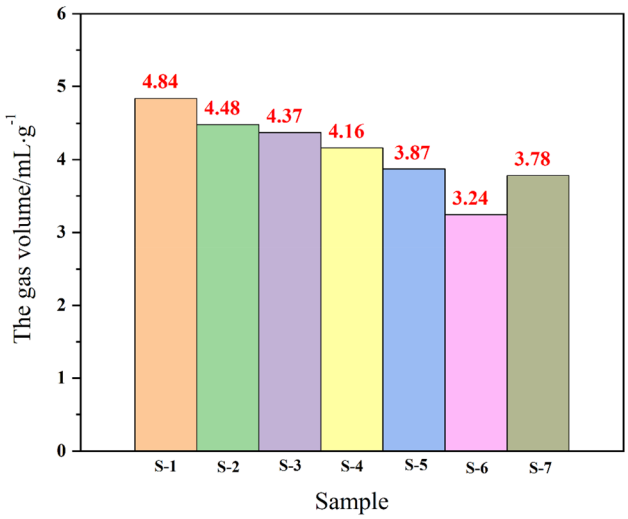

Fig. 5 Outgassing volumes of vacuum stabilization effect test samples.

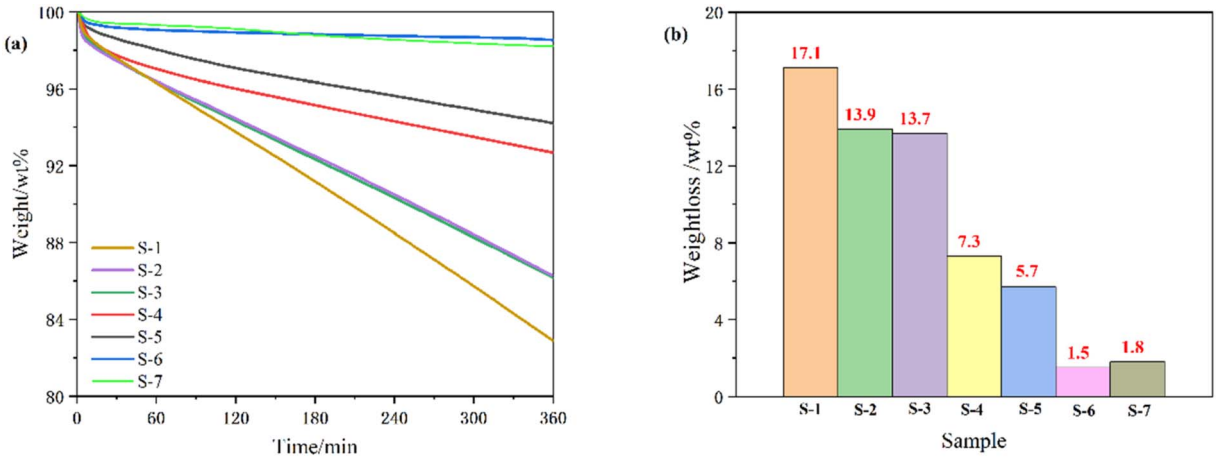

Fig. 6 (a) Weight loss curves and (b) final weight loss rate of the loss test samples.

by P (Pa), the reactor volume is expressed by V_0 (mL), the sample volume is expressed by V_G (mL), and the experimental temperature is expressed by T (K). The detailed results are shown in Fig. 5. The gas released by per unit mass of S-1–S-7 was 4.84, 4.48, 4.37, 4.16, 3.87, 3.24, and 3.78 mL g^{-1}, respectively. Therefore, the stabilizing ability of stabilizers on NC is **2c** > **2d** > **2b** > **2a** > C2 > DPA, and the experimental results reveal that C_{60}-CM-C_n has better stabilizing performance than C2 and DPA.

3.3.3. TG test. The TG test was conducted to assess the stabilization effect of the respective stabilizers by measuring the mass loss of samples under experimental conditions. A higher remaining weight rate indicates a more effective stabilizer.

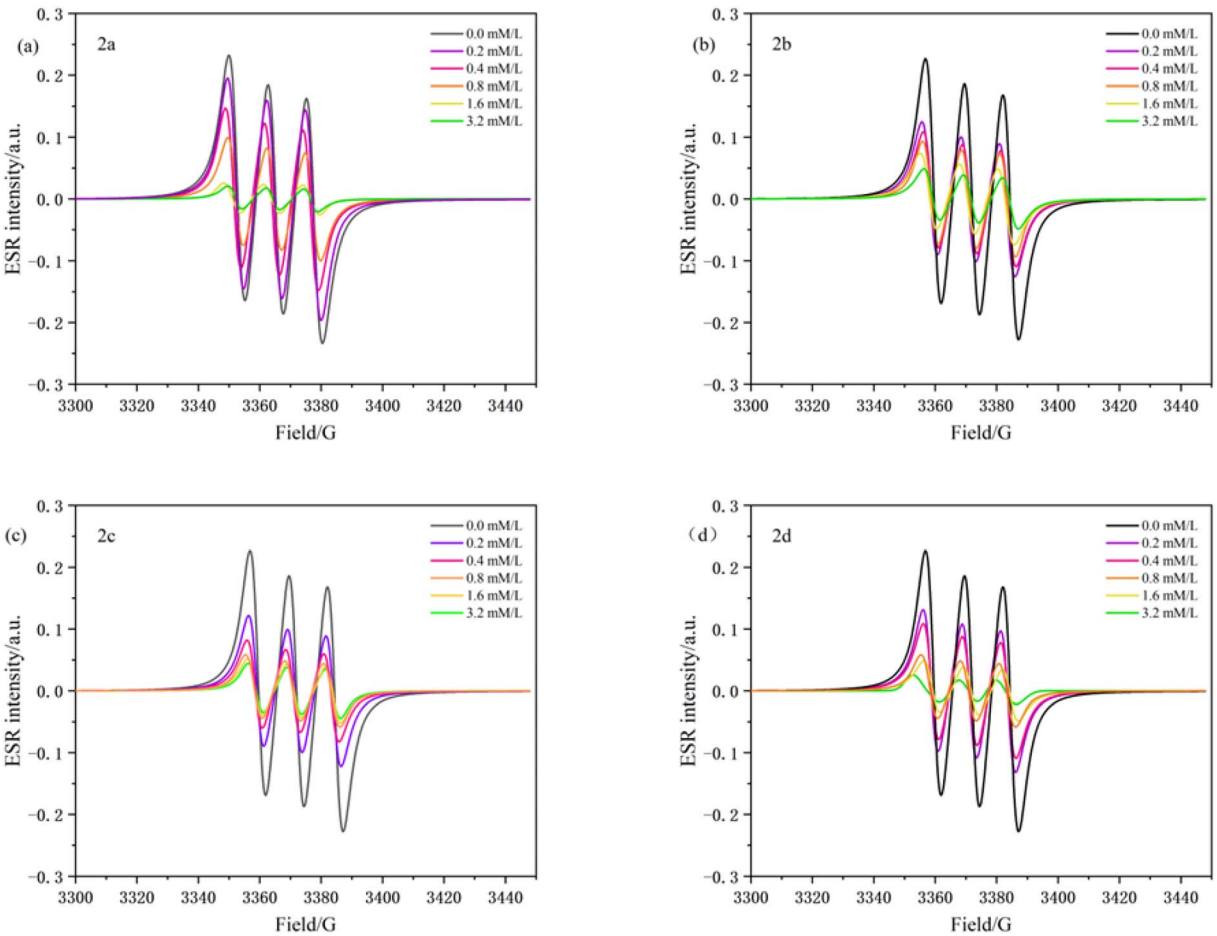

Fig. 7 The fullerene derivative C_{60}-CM-C_n.

Fig. 6 illustrates the weight retention curve and final weight residue for all samples. The weight loss rates for samples S-1 through S-7 were recorded as 17.1%, 13.9%, 13.7%, 7.3%, 5.7%, 1.5%, and 1.8%. Thus, the stabilization effects of these samples exceed those of conventional stabilizers.

3.4. Stabilization effect mechanism

3.4.1. ESR test. To explore the stabilization mechanism of NC using fullerene-based stabilizers, the absorption capacity of compounds **2a–2d** and C_{60} for NO radicals was investigated using the ESR method. Samples lacking compounds **2a–2d** and C_{60} displayed significantly stronger NO· ESR signals compared to those containing these compounds. Additionally, samples with higher concentrations of compounds **2a–d** and C_{60} exhibited lower NO· ESR signal intensities than those with lower concentrations. The radical scavenging abilities of the various compounds were assessed by comparing the intensity of their ESR absorption peaks under identical concentration conditions.[35] The test results for compounds **2a–d** are displayed in Fig. 7a–d. A high absorption intensity indicates a low capability to scavenge free radicals. The ESR curves for compounds **2a–2d** and C_{60} at 3.2 mM L^{-1} are shown in Fig. 8a. The absorption peak intensities of **2a–d** and C_{60} ranked as follows: **2c** < **2d** < **2b** < **2a** < C_{60} < blank samples. The equations for estimation of NO scavenging rate of **2a-1d** and C_{60} are as follows:

$$X = (I_0 - I_C)/I_0 \quad (2)$$

where the NO· clearance rate was expressed as X (%), the ESR signal intensity of the blank sample was expressed as I_0, and the EPR signal intensity of NO· after the addition of compounds **2a–2d** and C_{60} was expressed as I_C. The NO· scavenging rates of **2a–2d** and C_{60} at these concentrations (0.2, 0.4, 0.8, 1.6, and 3.2 mM L^{-1}) followed the order **2c** > **2d** > **2b** > **2a** > C_{60}. As shown in Fig. 8b and c. The IC_{50} (half-maximal inhibitive concentration) of compounds **2a–2d** and C_{60} were calculated to compare their ability to absorb NO·. The smaller the IC_{50} value of the compound, the stronger the absorption capacity of NO·. As shown in Fig. 8d, the IC_{50} values of compounds **2a–2d** and C_{60} for the NO· scavenging rates were 0.8802, 0.6180, 0.4119, 0.1901, and 0.3807 mM L^{-1}, respectively. The IC_{50} values of compounds **2a–2d** and C_{60} for the NO· scavenging rates had the following order **2c** < **2d** < **2b** < **2a** < C_{60}. Therefore, the ESR results show that compounds **2a–d** all have the ability to absorb

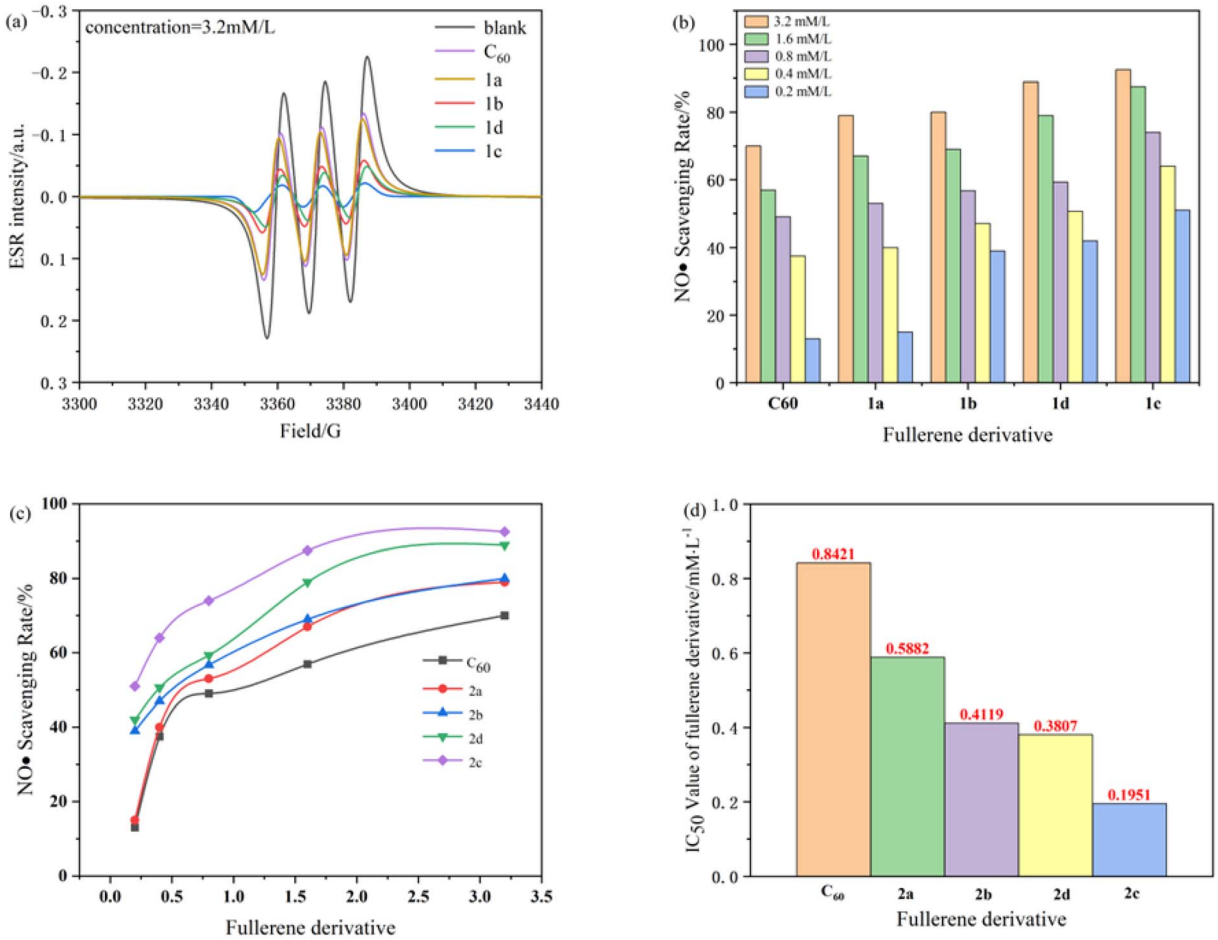

Fig. 8 (a) The ESR curves of compounds **2a–2d** and C_{60} at the 3.2 mM L^{-1} and blank sample; (b and c) NO· scavenging rates of compounds **2a–2d** and C_{60}; (d) IC_{50} values of compounds **2a–2d** and C_{60} for the NO· scavenging rates.

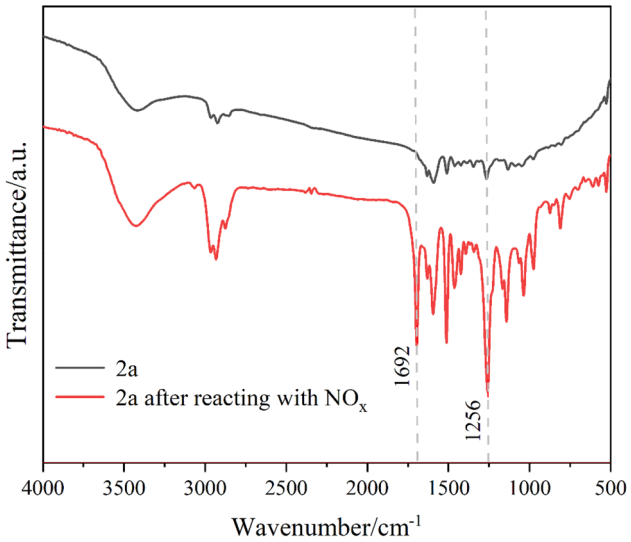

Fig. 9 FT-IR spectra of products **2a** before and after interaction with NC.

nitro radicals and are greater than C_{60}, supporting the results of the stabilizing effect test.

3.4.2. FT-IR test. The experiment takes compound **2a** as an example. After the stability of sample S-4 was demonstrated, solvent was used to extract **2a** after interacting with NC for infrared analysis, and compared with pure **2a**. The FT-IR spectra of compound **2a** and nitrogen oxides absorbed from NC decomposition are shown in Fig. 9. New strong $^{23}NO_2$ vibrational peaks were discovered at 1692 and 1256 cm^{-1}. These results indicate that fullerene derivative **2a** interacts chemically with acidic nitrogen oxides, inhibiting the self catalytic decomposition of NC.

4. Conclusion

This paper reports the successful synthesis of four C_{60}-CM-C_n compounds through a binge reaction. The structures of these compounds were confirmed using ^{1}H NMR, ^{13}C NMR, and HRMS techniques. The compatibility and stabilizing effects of the compounds in NC were evaluated using VST, methyl violet, TG, DTA, and ESR test methods. The stabilizing effect results demonstrated that **2c** exhibited superior stabilization (**2c** > **2d** > **2b** > **2a**) compared to C_{60} and conventional stabilizers. The C_{60}-CM-C_n compounds showed enhanced stabilization. To further investigate the stabilization mechanism of fullerene pyrrolidine derivatives on NC, w detailed characterization was conducted using ESR tests. The findings indicated that the ability to absorb nitro radicals followed the order: **2c** > **2d** > **2b** > **2a** > C_{60}. This supports the stabilizing effect results, confirming that all four C_{60}-CM-C_n compounds possess a greater ability to absorb nitro radicals than C_{60}. Experiments have shown that the new fullerene based stabilizer can extend the service life of solid propellants, improve the safety level during use, and its performance is superior to traditional stabilizers. Considering the potential of new fullerene derivatives to replace traditional chemical stabilizers, we will continue to explore the practical applications of these fullerene based stabilizers in the future.

Data availability

All relevant data are within the manuscript and its additional files.

Conflicts of interest

There are no conflicts of interest to declare.

Acknowledgements

This work was supported by the financial support received from the National Natural Science Foundation of China (22305196), and Open Project of State Key Laboratory of Environment-friendly Energy Materials, Southwest University of Science and Technology (No. 19fksy04).

References

1 W. Q. Pang, X. Z. Fan, J. H. Yi, F. Q. Zhao, H. X. Xu, J. Z. Li, B. Z. Wang and Y. H. Li, *Chin. J. Chem.*, 2010, **28**, 687–692.
2 E. Morris, C. R. Pulham and C. A. MOrrison, *RSC Adv.*, 2023, **13**(46), 32054–32841.
3 M. R. Sovizi, S. S. Hajimirsadeghi and B. Naderizadeh, *J. Hazard. Mater.*, 2009, **168**, 1134–1139.
4 S. Guo, Q. S. Wang, J. H. Sun, X. Liao and Z. S. Wang, *J. Hazard. Mater.*, 2009, **168**, 536–541.
5 B. P. Mason and C. M. Roland, *Rubber Chem. Technol.*, 2019, **92**, 1–24.
6 M. Suceska, S. M. Musanic and I. F. Houra, *Thermochim. Acta*, 2010, **510**, 9–16.
7 L. S. Lussier, H. Gagnon and M. A. Bohn, *Propellants, Explos., Pyrotech.*, 2000, **25**, 117–125.
8 N. J. Curtis and P. E. Rogasch, *Propellants, Explos., Pyrotech.*, 2004, **12**, 158–163.
9 E. Tirak, M. Moniruzzaman, E. Degirmenci and A. Hameed, *Thermochim. Acta*, 2019, **680**, 9.
10 D. Trache and A. F. Tarchoun, *J. Mater. Sci.*, 2017, **53**, 100–123.
11 Y.-x. Li, W.-t. Yang and S.-j. Ying, *Def. Technol.*, 2014, **10**, 261–268.
12 S. Chelouche, D. Trache, A. F. Tarchoun, K. Khimeche and A. Mezroua, *J. Therm. Anal. Calorim.*, 2019, **141**, 941–955.
13 S. Wilker, G. Heeb, B. Vogelsanger, J. Petržílek and J. Skládal, *Propellants, Explos., Pyrotech.*, 2007, **32**, 135–148.
14 W. A. Schroeder, B. Keilin and R. M. Lemmon, *Ind. Eng. Chem.*, 1951, **43**, 939–956.
15 X. Chang, Y. Xu and M. von Delius, *Chem. Soc. Rev.*, 2024, **53**, 47–83.
16 M. C. Tsai, Y. H. Chen and L. Y. Chiang, *J. Pharm. Pharmacol.*, 1997, **49**, 438–445.
17 S. C. Chueh, M. K. Lai, M. S. Lee, L. Y. Chiang, T. I. Ho and S. C. Chen, *Transplant. Proc.*, 1999, **31**, 1976–1977.

18 T. Lindblom, *Propellants, Explos., Pyrotech.*, 2002, **27**, 197–208.
19 P. J. Krusic, E. Wasserman, P. N. Keizer, J. R. Morton and K. F. Preston, *Science*, 1991, **254**, 1183–1185.
20 M. Q. Chen, R. N. Guan and S. F. Yang, *Adv. Sci.*, 2019, **6**, 26.
21 E. A. Khakina and P. A. Troshin, *Russ. Chem. Rev.*, 2017, **86**, 805–830.
22 Y. Zhao, B. Jin, R. F. Peng and L. Ding, *Cellulose*, 2020, **27**, 3611–3622.
23 G. Li, B. Jin, Z. H. Chai, L. Ding, S. J. Chu and R. F. Peng, *Polym. Degrad. Stab.*, 2020, **172**, 9.
24 L. Liao, B. Jin, Z. C. Guo, F. Xian, C. J. Hou and R. F. Peng, *Def. Technol.*, 2021, **17**, 1944–1953.
25 P. R. Birkett, A. G. Avent, A. D. Darwish, H. W. Kroto, R. Taylor and D. R. M. Walton, *J. Chem. Soc., Chem. Commun.*, 1995, 683–684, DOI: **10.1039/c39950000683**.
26 J. L. Nascimento Mossri, R. L. Barboza Rodrigues, J. Nichele and I. Borges Jr, *ChemRxiv*, 2023, **42**(5), DOI: **10.26434/chemrxiv-2023-dwwdt**.
27 R. L. B. Rodrigues, P. A. Gomes Buitrago, N. L. Nakano, F. C. Peixoto, M. F. Lemos, T. C. C. França and L. G. Mendonça Filho, *J. Energ. Mater.*, 2021, **40**, 218–241.
28 W. B. Huang, C. Y. Du, J. A. Jiang and Y. F. Ji, *Res. Chem. Intermed.*, 2013, **39**, 2849–2856.
29 D. Milic and M. Prato, *Eur. J. Org Chem.*, 2010, **2010**, 476–483.
30 Q. Lu, I. D. Schuster and R. S. Wilson, *J. Org. Chem.*, 1996, **61**, 4764–4768.
31 S. Bosi, L. Feruglio, D. Milic and M. Prato, *Eur. J. Org Chem.*, 2003, **2003**, 4741–4747.
32 Y. Qi-Long, L. Xiao-Jiang, Z. La-Ying, L. Ji-Zhen, L. Hong-Li and L. Zi-Ru, *J. Hazard. Mater.*, 2008, **160**, 529–534.
33 C. Salim, D. Trache, A. F. Tarchoun, A. Abdelaziz and K. Khimeche, *J. Energ. Mater.*, 2020, **38**, 48–67.
34 C. Salim, D. Trache, A. F. Tarchoun, A. Abdelaziz and K. Khimeche, *J. Therm. Anal. Calorim.*, 2020, **141**, 941–955.
35 V. V. Novikov, A. A. Pavlov, J. Nehrkorn and Y. V. Nelyubina, *Russ. J. Coord. Chem.*, 2020, **46**, 756–761.